AIAA JOURNAL
Vol. 43, No. 9, September 2005

Fracture Analysis of Stiffened Panels Under Combined Tensile, Bending, and Shear Loads

G. S. Palani* and Nagesh R. Iyer†
Structural Engineering Research Centre, Chennai 600 113, India
and
B. Dattaguru‡
Indian Institute of Science, Bangalore 560 012, India

The objective is to present the formulation of numerically integrated modified virtual crack closure integral technique for concentrically and eccentrically stiffened panels for computation of strain-energy release rate and stress intensity factor based on linear elastic fracture mechanics principles. Fracture analysis of cracked stiffened panels under combined tensile, bending, and shear loads has been conducted by employing the stiffened plate/shell finite element model, MQL9S2. This model can be used to analyze plates with arbitrarily located concentric/eccentric stiffeners, without increasing the total number of degrees of freedom of the plate element. Parametric studies on fracture analysis of stiffened plates under combined tensile and moment loads have been conducted. Based on the results of parametric studies, polynomial curve fitting has been carried out to get best-fit equations corresponding to each of the stiffener positions. These equations can be used for computation of stress intensity factor for cracked stiffened plates subjected to tensile and moment loads for a given plate size, stiffener configuration, and stiffener position without conducting finite element analysis.

Nomenclature

A_p	=	cross-section area of plate
A_s	=	cross-section area of stiffeners
$a_0, a_1, \ldots, a_{(n-1)}$	=	polynomial coefficients associated with displacements/rotations
$b_0, b_1, \ldots, b_{(n-1)}$	=	polynomial coefficients associated with forces/moments
E	=	Young's modulus
$F_{y,j}$, $F_{y,j+1}$, etc., or $M_{y,j}$, $M_{y,j+1}$, etc.	=	forces or moments at the nodes j, $j+1$, etc.
G	=	strain-energy release rate
G_{I} and G_{II}	=	G for in-plane modes I and II, respectively
G_1, G_2, and G_3	=	G for out-of-plane modes 1, 2, and 3 respectively
H, W	=	height and width of plate
I_p	=	moment of inertia of cross section of plate
I_s	=	moment of inertia of cross section of stiffeners
$[K_p]$	=	plate element stiffness matrix
$[K_s]$	=	stiffness matrix for an arbitrarily located eccentric stiffener
K_{I} and K_{II}	=	stress intensity factor for in-plane modes I and II, respectively
k_1, k_2, and k_3	=	stress intensity factor for out-of-plane modes 1, 2, and 3, respectively
$N_i(\xi)$	=	shape functions for three-noded beam element
$N_i(\xi, \eta)$	=	shape functions for nine-noded plate element
N_p and N_s	=	total number of plate and stiffener elements, respectively
P	=	concentrated forces or moments
q	=	uniform loading acting normal to the element surface or along the element edges
$[T_{\mathrm{cp}}]$	=	transformation matrix, which takes care of the arbitrary position of the stiffeners in the plate element
$[T_e]$	=	transformation to account for the eccentricity of stiffeners
t	=	plate thickness
t_s and d_s	=	thickness and depth of stiffener
U_x and U_y	=	relative sliding and opening displacements between the crack faces
U_z	=	relative out-of-plane displacement between the crack faces
Δa	=	virtual crack increment
ν	=	Poisson's ratio
σ_{yy} and σ_{xy}	=	in-plane stress components
σ_{yz}	=	out-of-plane stress component
$2a$	=	crack length

Introduction

MANY industrial structures such as aerospace structures, ship hulls, and offshore platforms are generally made up of stiffened-plate/shell panels. The strength of thin-plate structural components is generally improved by appropriately using the stiffening members such as stiffeners/stringers or more generally by judicious use of thicker or paneled sections for crack-growth retardation/arrest. Such a control of crack growth is one of the very important parameters[1] for consideration of damage-tolerant design and failure assessment of structures and structural components. When modeling these complex structural components for the purpose of fracture analysis by using the finite element method (FEM), one might have to deal with arbitrarily located eccentric stiffeners. The problem is highly indeterminate, and the question arises as to what is the best way of modeling them for fracture analysis. Also the postprocessing technique for the estimation of stress intensity factor (SIF) needs to be selected appropriately. Therefore, studies on the behavior of cracked-stiffened structures have assumed great importance.

Received 21 July 2004; revision received 11 March 2005; accepted for publication 2 April 2005.

*Scientist, CSIR Campus, Taramani; pal@sercm.csir.res.in.
†Director Grade Scientist, CSIR Campus, Taramani.
‡Professor Emeritus.

Configurations involving cracks in infinite sheets, subjected to uniaxial tensile stresses, reinforced with continuously attached (bonded or integral) or discretely attached (riveted) stiffeners were studied by several authors.[2–7] It is an important requirement to study the influence of the various parameters such as stiffener size, spacing, and load transmission characteristics on SIF in these panels. Isida[8] made extensive use of series representation of complex functions for problems involving cracks in stiffened sheets. Poe[9] made a complete study on the influence of geometry parameters on SIF for cracked-stiffened panels. The sheet was modeled as an infinite plate with a crack. The influence of crack spacing, rivet spacing, and stringer spacing was studied by various workers for a stiffened panel with a symmetric crack distribution.

Shkarayev and Moyer[3] proposed an analytical method for the determination of SIF for edge cracks in stiffened panels. The analytical solution for a semi-infinite plate containing an edge crack is employed in the modeling. Utukuri and Cartwright[5] presented procedures for application of complex variable method combined with compatible deformations for fracture analysis of finite multiply stiffened panels. The effect of attachment forces was represented as traction boundary conditions on the edges of the panel. The resulting nonlinear system of equations was solved using a least-squares iterative scheme. SIFs were computed for several multiply stiffened configurations and found to be in good agreement with the existing solutions. Wu and Cartwright[10] reduced the preceding problem to the direct solution of a system of linear equations and extended the method to solve problems involving cracks emanating from internal boundaries in multiply stiffened sheets. Yashi and Shahid[11] obtained the analytical solution for a stiffened plate containing a through-crack under uniform bending load by using Reissner's plate theory and the Fourier integral transform technique. The asymptotic stress state near the crack tip terminating at the stiffener was examined, and it was shown that the order of singularity at the crack tip adjacent to the stiffener is independent of the stiffener properties and is a function of only Poisson's ratio of the material. They have also shown that the existence of the stiffener has considerable effect on SIF. Recently, Yeh and Kulak[12] proposed procedures for evaluation of SIF and energy release rate for cracked orthotropic sheets with riveted stiffeners. An approach based on compatibility of displacements among the sheet, fasteners, and stiffeners was used to obtain closed-form solutions for SIF. Collins et al.[13] presented procedures for the analysis of stiffened panel structures containing multiple site damage through the complex variable method in association with the requirement for displacement compatibility. The method is extended by replacing the usual single crack stress and displacement functions by those for a series of arbitrary straight collinear cracks, which are used to model exactly the main and secondary crack damage in the sheet. It is shown that the problem can be reduced to a system of linear equations for the unknown forces at the attachment points between the sheet and the stiffener from which SIF of the collinear cracks can be determined. The advantage of the analytical methods is that they allow parametric studies to be performed relatively easily. However, this usually requires some simplifications to be made that involve relatively complex geometries or loading conditions before they can be analyzed. In general, structural components have complex shapes, and cracks tend to occur in regions of high stress concentration, such as corners, cut-outs, edges, change in curvature, surfaces with high gradients, doubly curved surfaces, etc. In view of these, it is frequently necessary to use numerical methods of structural analysis for solving problems of cracked stiffened panels that can represent geometry as accurately.

The problem of fracture analysis of cracked-stiffened panels has been studied by using matrix method of structural analysis and FEM.[1,14–16] Swift[14] used the matrix force method to analyze cracked-stiffened panels. The panels were modeled by using bar and shear elements. Stiffener elements were represented by additional bars lumped to the panel or connected by shear elements. The opening of a straight crack was simulated by successively releasing displacement constraints. Swift[17] also proposed a method based on displacement compatibility for fracture analysis of cracked-stiffened panels. Emphasis was placed on the need to account for stiffener bending stresses in residual strength calculations. A methodology based on fastener nonlinear shear displacements was proposed, which can account for the effect of fastener failure during the failure process of a cracked-stiffened panel. The method can be effectively used for determination of crack-tip SIF and stiffener stress concentration factors that can be used for crack growth and residual strength studies. The method was based on superposition of various exact mathematical solutions for the deformations and SIF in an unstiffened cracked skin under various loads. Zaal et al.[18] modified the governing equations for the displacement compatibility method such that the stiffener deformations are described by using the stiffness matrix.

The problem of fracture analysis of stiffened panels is strictly three-dimensional in nature. However, it is generally reduced to a two-dimensional problem by using appropriate plate and beam theories. Hence, two-dimensional finite elements can be effectively employed in conducting the fracture analysis of stiffened panels. Vlieger[6] analyzed a finite panel with riveted stiffeners and a crack by using FEM and calculated SIF from strain-energy release rate (SERR). Ratwani and Wilhem[2] carried out the elastic and elasto-plastic analysis of a biaxially loaded stiffened panel by using FEM. The elasto-plastic analysis was accomplished assuming Prandtl–Reuss material behavior. The influence of biaxial load ratios on crack openings, stresses in the stringer, plastic zone size, and $\sqrt{J}$ was studied. It was observed that contrary to the behavior of unstiffened structure, the $\sqrt{J}$ values and crack openings increase for positive biaxial load ratios in stiffened structures. Shkarayev and Moyer[3] employed special crack-tip enriched finite element to solve problems involving edge cracks in stiffened panels. The finite element solution reported[3] was within 6% of the analytical results. Shkarayev and Moyer[4] also proposed methodologies for evaluation of SIFs in modes I and II for cracked-stiffened panels loaded both in tension and shear by using FEM. The influence of stringer thickness, rivet spacing, and stringer stresses were analyzed.

Dowrick et al.[19] and Young et al.[15,20] used the boundary element method to solve problems involving continuously and discretely attached stiffeners. In the work reported, the method of compatible deformations was used to combine the boundary integral displacement equations of the plate with the stiffener displacement equation. The presence of a straight crack was implicitly considered by using Green's function specially proposed to account for cracks. This feature, although it avoids the need for modeling the crack geometry, restricts the application to problems involving a straight crack. Salgado and Aliabadi[21] presented procedures based on the dual boundary element method to the analysis of cracked-stiffened panels with continuously and discretely attached stiffeners. Displacement compatibility between the plate and the stiffeners was imposed in the formulations. The J-integral technique was used to compute SIF. Wen et al.[7] presented coupled dual boundary integral equations based on the shear deformable plate theory for stiffened-cracked plates. The boundary values of rotations and deflections for shear deformable plate were determined by solving boundary integral equations numerically. SIF for both the tensile and bending loads were obtained by using the crack-opening displacements.

It is observed that the analytical methodologies for fracture analysis of stiffened plates generally deals with mode I loading and accounts for the case of concentric stiffeners. There is a need to account for eccentricity of stiffeners with respect to the midsurface of the plates. The methodologies available to address the problem of fracture analysis of cracked-stiffened plates subjected to general loading conditions are not adequate. Therefore, there is scope for improvement of these procedures by employing appropriate stiffened-plate finite element models in conducting the fracture analysis. In this context the modified virtual crack closure integral (MVCCI) technique for fracture analysis of cracked-stiffened plates subjected to tensile, bending, and shear loads can be the most appropriate. However, it is observed from the literature that this technique has not been applied and investigated for stiffened panels.

In this paper the numerically integrated modified virtual crack closure integral (NI-MVCCI) technique, a generalized and element independent MVCCI technique, for fracture analysis of

cracked-stiffened plates subjected to tensile, bending, and shear loads has been presented. It is observed from the studies conducted on the fracture analysis of plates[22] that the performance of a nine-noded Lagragian element with assumed shear strain field exhibit better performance among other quadrilateral plate elements considered. In this paper this element has been appropriately combined with three-noded beam element for formulating the MQL9S2 stiffened-plate finite element model. The plate and the stiffener elements are based on Reissner–Mindlin plate theory and Timoshenko beam theory, respectively, which accounts for shear deformations. Parametric studies on fracture analysis of stiffened panels subjected to tension-moment loads have been conducted employing these elements.

Formulation of Stiffened Plate Finite Element Model

A more realistic finite element model of stiffened plates is achieved by considering the plate and stiffeners separately and by maintaining the compatibility between the two. Extensive studies have been conducted by Palani et al.[23] to identify efficient plate and stiffener elements, and the authors of this reference have proposed QL9S2 model (nine-noded biquadratic Lagrangian plate element combined with three-noded eccentric and arbitrarily located stiffener element) for static and dynamic analysis of stiffened plates. The stiffened plate finite element model QL9S2 is formulated[24,25] by combining nine-noded plate element with three-noded isoparametric stiffener element. This model can be used to analyze plates with arbitrarily located concentric/eccentric stiffeners, without increasing the total number of degrees of freedom of the plate element. In the following formulation, an improved version of QL9S2 finite element model, that is, MQL9S2, has been presented in which a nine-noded Lagrangian plate element has been replaced with a nine-noded Lagrangian plate element with assumed transverse shear strain fields.[26] The formulation of MQL9S2 model has been presented briefly in the following. The subscripts p and s in the following refer to plate and stiffener, respectively. The displacement field for the plate elements (Fig. 1) (with five degrees of freedom at each node) can be expressed as

$$\phi_p = \begin{Bmatrix} U_{\mathrm{xp}} \\ U_{\mathrm{yp}} \\ U_{\mathrm{zp}} \\ \theta_{\mathrm{xp}} \\ \theta_{\mathrm{yp}} \end{Bmatrix} = \sum_{i=1}^{n_p} N_i(\xi, \eta) I_p \delta_{\mathrm{pi}} \tag{1}$$

where $N_i(\xi, \eta)$ are the shape functions for nine-noded element and I_p is a 5×5 identity matrix.

The displacement field for three-noded stiffener element (with four degrees of freedom at each node) can be expressed as

$$\begin{Bmatrix} U_{\mathrm{xs}} \\ U_{\mathrm{zs}} \\ \theta_{\mathrm{xs}} \\ \theta_{\mathrm{ys}} \end{Bmatrix} = \sum_{i=1}^{3} N_i(\xi) I_s \delta_{\mathrm{si}} \tag{2}$$

where $N_i(\xi)$ are the shape functions for three-noded beam element and I_s is a 4×4 identity matrix. For an arbitrarily located eccentric stiffener (Fig. 1), the stiffener nodal degrees of freedom can be transformed to the plate nodal degrees of freedom using the relationship

$$\{\delta_s\} = [T_e][T_{\mathrm{cp}}]\{\delta_p\} \tag{3}$$

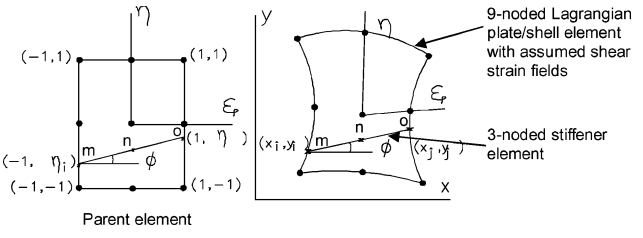

Fig. 1 Arbitrarily located stiffened plate/shell model (MQL9S2).

The details of the transformation as given in Eq. (3) are provided by Palani et al.[24,25] It can be observed that degrees of freedom of the element have not increased.

With the use of the principle of virtual work, the equilibrium equations can be expressed as

$$\sum^{N_p} \int_A \partial \varepsilon_p^T \sigma_p \, \mathrm{d}A + \sum^{N_s} \int_{\mathrm{I}} \partial \varepsilon_s^T \sigma_s \, \mathrm{d}x = \sum^{Np} \int_A \partial \phi_p^T q \, \mathrm{d}A + \sum^{Np} \int_1 \partial \phi_p^T P \tag{4}$$

Substituting $\varepsilon_p = B_p \delta_p$, $\sigma_p = D_p B_p \delta_p$, $\varepsilon_s = B_s \delta_s$, $\sigma_s = D_s B_s \delta_s$, and for $\{\delta_s\}$ from Eq. (3) and on simplification

$$\sum^{Np} \int_A \partial \delta_p^T [K_p] \delta_p \, \mathrm{d}A + \sum^{Ns} \int_1 \partial \delta_p^T [K_s] \delta p \, \mathrm{d}x = \sum^{Np} \int_A \partial \delta_p^T N^T q \, \mathrm{d}A + \sum^{Np} \int_1 \partial \delta^T N^T P \tag{5}$$

where

$$[K_p] = \int_A B_p^T D_p B_p \, \mathrm{d}A$$

is the plate element stiffness matrix,

$$[K_s] = T_{\mathrm{cp}}^T T_e^T \left[\int_1 B_s^T D_s B_s \, \mathrm{d}x \right] T_e T_{\mathrm{cp}}$$

is the stiffness matrix for an arbitrarily located eccentric stiffener. The plate element stiffness matrices are evaluated employing an nine-noded Lagrangian element with assumed shear strain fields with full integration, and the stiffness matrices for the stiffener elements are evaluated employing three-noded beam element with reduced integration technique.

NI-MVCCI Technique for Plates Under Combined Tensile, Bending, and Shear Loads

Irwin[27] proposed a crack closure integral (CCI) technique for the estimation of G. CCI for evaluation of SERR was derived by using a fundamental concept that when crack extension has taken place the energy required to close this part of crack in a solid is the same as the strain-energy release during the crack extension. The rate of change of this strain energy with crack extension is SERR. Figure 2 shows a crack tip in an infinite isotropic media subjected to remote tensile and bending loads causing tensile mode-I and bending mode-1 fracture. For plates subjected to tensile and bending loads, the stresses on a plane ahead of the crack $\theta = 0$ are given in terms of SIF by Sih[28] as

$$\sigma_{yy}(r, \theta = 0) = \frac{K_{\mathrm{I}}}{\sqrt{2\pi r}} + \frac{k_1}{\sqrt{2r}} \frac{2z}{t}$$

$$\sigma_{xy}(r, \theta = 0) = \frac{K_{\mathrm{II}}}{\sqrt{2\pi r}} + \frac{k_2}{\sqrt{2r}} \left(\frac{1+\nu}{3+\nu} \right) \frac{2z}{t}$$

$$\sigma_{yz}(r, \theta = 0) = \frac{-k_2 h}{2(2r)^{\frac{3}{2}}(3+\nu)} \left[1 - \left(\frac{2z}{t} \right)^2 \right] \tag{6}$$

The in-plane stress components σ_{yy} and σ_{xy} have a constant term resulting from the in-plane loads and a linearly varying term resulting from the bending loads. The out-of-plane stress component σ_{yz} is caused by the bending loads and varies parabolically through the thickness of the plate.

For a linearly elastic plate of thickness t, SERR for self-similar extension of a through crack lying in the x–y plane can be expressed

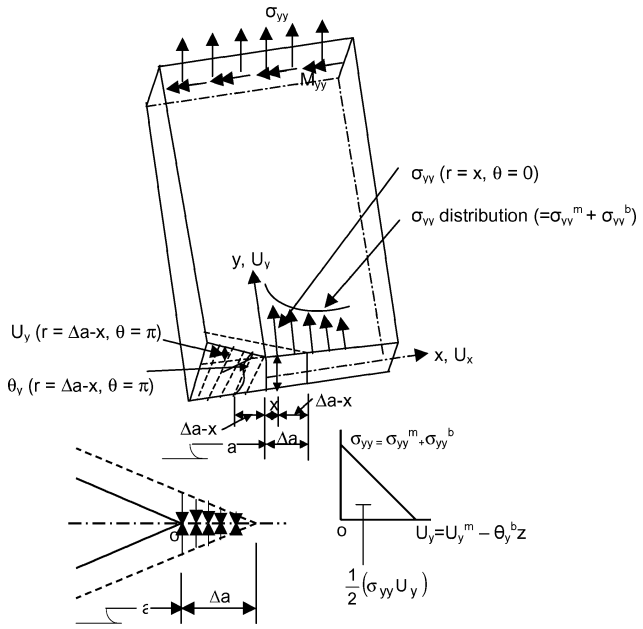

Fig. 2 Schematic of virtual crack extension under bending loads.

as[27]

$$G = \lim_{\Delta a \to 0} \frac{1}{2t\Delta a} \int_0^{\Delta a} \int_{-t/2}^{t/2} [\sigma_{xy}(x, \theta = 0) U_x(\Delta a - x, \theta = \pi) + \sigma_{yy}(x, \theta = 0) U_y(\Delta a - x, \theta = \pi) + \sigma_{yz}(x, \theta = 0) U_z(\Delta a - x, \theta = \pi)] \, dz \, dx \tag{7}$$

where $\sigma_{yy}(r = x, \theta = 0)$, $\sigma_{xy}(r = x, \theta = 0)$, and $\sigma_{yz}(r = x, \theta = 0)$ are distributions of stresses ahead of the crack tip. $U_x(r = \Delta a - x, \theta = \pi)$ and $U_y(r = \Delta a - x, \theta = \pi)$ are the relative sliding and opening displacements between the crack faces. $U_z(r = \Delta a - x, \theta = \pi)$ is the out-of-plane displacement between the crack faces.

The displacement and stress components can be expressed in terms contribution caused by tensile and bending loads as

$$\sigma_{xy} = \sigma_{xy}^m + \sigma_{xy}^b, \qquad U_x = U_x^m - \theta_x^b z$$
$$\sigma_{yy} = \sigma_{yy}^m + \sigma_{yy}^b, \qquad U_y = U_y^m - \theta_y^b z$$
$$\sigma_{yz} = \sigma_{yz}^b, \qquad U_z = U_z^b \tag{8}$$

The subscripts m and b represent the corresponding displacement and stress components that are caused by tensile and bending loads, respectively. It can be noted that membrane portion is constant through the thickness, whereas the bending portion has linear variation (linear in z) through the thickness. Substituting for the displacement and stress fields given by Eq. (8) in Eq. (7), SERR can be expressed as

$$G = \lim_{\Delta a \to 0} \frac{1}{2t\Delta a} \int_0^{\Delta a} \int_{-t/2}^{t/2} \left[\sigma_{xy}^m(x, \theta = 0) U_x^m(\Delta a - x, \theta = \pi) + \sigma_{yy}^m(x, \theta = 0) U_y^m(\Delta a - x, \theta = \pi) + \sigma_{xy}^b(x, \theta = 0) z\left[-\theta_x^b(\Delta a - x, \theta = \pi)\right] + \sigma_{yy}^b(x, \theta = 0) z\left[-\theta_y^b(\Delta a - x, \theta = \pi)\right] + \sigma_{yz}^b(x, \theta = 0) U_z^b(\Delta a - x, \theta = \pi)\right] dz \, dx \tag{9}$$

The terms of the integrand in Eq. (9) that are linear in z integrate to zero through the thickness. This results in uncoupled membrane and bending portions in evaluation of SERR. After carrying out the integrals with respect to z and by substituting for bending stress components in terms of moment and shear stress resultants,

$$\sigma_{xy}^b = 12 M_{xy} z / t^3, \qquad \sigma_{yy}^b = 12 M_{yy} z / t^3$$
$$\sigma_{yz}^b = (3 Q_z / 2t)[1 - (2z/t)^2] \tag{10}$$

SERR can be expressed as

$$G = \lim_{\Delta a \to 0} \frac{1}{2\Delta a} \int_0^{\Delta a} \left(\sigma_{xy}^m U_x^m + \sigma_{yy}^m U_y^m - M_{xy}\theta_x - M_{yy}\theta_y + Q_z U_z\right) dx \tag{11}$$

The components of SERR can be expressed as

$$G_{\mathrm{I}} = \lim_{\Delta a \to 0} \frac{1}{2\Delta a} \int_{\Delta a} \sigma_{yy}^m U_y^m \, dx$$
$$G_{\mathrm{II}} = \lim_{\Delta a \to 0} \frac{1}{2\Delta a} \int_{\Delta a} \sigma_{xy}^m U_x^m \, dx \tag{12a}$$
$$G_1 = \lim_{\Delta a \to 0} \frac{1}{2\Delta a} \int_{\Delta a} M_y \theta_y \, dx$$
$$G_2 = \lim_{\Delta a \to 0} \frac{1}{2\Delta a} \int_{\Delta a} Q_z U_z \, dx$$
$$G_3 = \lim_{\Delta a \to 0} \frac{1}{2\Delta a} \int_{\Delta a} M_{xy} \theta_x \, dx \tag{12b}$$

and therefore, total SERR,

$$G_t = G_{\mathrm{I}} + G_{\mathrm{II}} + G_1 + G_2 + G_3 \tag{12c}$$

The five components of SERR can be related to the four SIF[29] as

$$G_{\mathrm{I}} = \frac{K_{\mathrm{I}}^2}{E}; \qquad G_{\mathrm{II}} = \frac{K_{\mathrm{II}}^2}{E} \tag{13a}$$
$$G_1 = \frac{k_1^2 \pi}{3E}\left(\frac{1+\nu}{3+\nu}\right)$$
$$G_2 + G_3 = \frac{k_2^2 \pi (1+\nu)^2}{3E(3+\nu)^2} + \frac{K_2^2 \pi 2(1+\nu)}{3E(3+\nu)^2} = \frac{k_2^2 \pi}{3E}\left(\frac{1+\nu}{3+\nu}\right) \tag{13b}$$

The objective of this paper is to employ NI-MVCCI technique involving numerical integration for computation of the constants and to perform the crack closure integrals for G_{I} and G_{II} and G_1 to G_3 as given by Eq. (12). NI-MVCCI is a generalized technique, and the expressions for computing SERR are independent of the type of finite element employed. The procedure for evaluating SERR for tensile mode I (G_{I}) and bending mode 1 (G_1) fracture is explained in the following. The same procedure can be used for evaluating other components of SERR as given by Eq. (12).

Consider a typical finite element mesh at the crack tip as shown in Fig. 3. For tensile mode-I and bending mode-1 fracture, G_{I} and

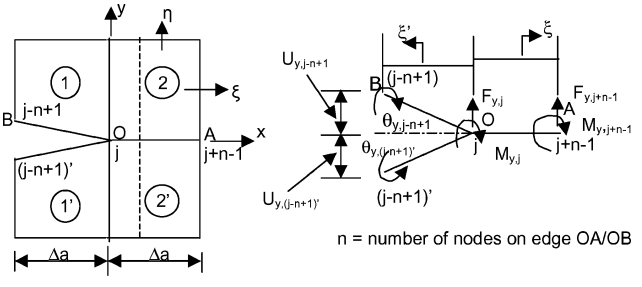

Fig. 3 Typical finite element mesh of crack-tip region with a stiffener.

G_1 can be evaluated by multiplying the stress/moment distribution along OA (ahead of crack tip) with the corresponding displacement/rotation distribution along OB (behind crack tip) and integrating this product over Δa. For evaluation of G_1 and G_1, stress/moment distribution on the crack extension line OA is expressed in terms of the nodal forces $F_{y,j}$, $F_{y,j+1}$, etc. or $M_{y,j}$, $M_{y,j+1}$ acting at the nodes $j, j+1$, etc., respectively. The crack-opening displacement/rotation distribution along OB is expressed in terms of the nodal values at j, $j-1$, $(j-1)'$, etc. G_1 and G_1 are derived by evaluating the energy required to close the crack over a length Δa in terms of these nodal forces/moments and displacements/rotations. The shape functions in elements 1 and 2 along OB can be obtained by substituting $\eta = -1$, in the respective element shape functions N_i.

The displacement/rotation distribution along OB can be expressed in terms of nodal displacements $\{(U_y)_i\}$ and rotations $\{(\theta_y)_i\}$ as

$$U_y = [N_i]\{(U_y)_i\}, \qquad i = 1, 2, \ldots, n \tag{14a}$$

$$\theta_y = [N_i]\{(\theta_y)_i\}, \qquad i = 1, 2, \ldots, n \tag{14b}$$

where n is the number of nodes on the edge OB of the element. Consistent with the isoparametric formulation, coordinate of any point $X(x, y)$ is given by

$$X = [N_i]\{(X)_i\}, \qquad i = 1, 2, \ldots, n \tag{15}$$

where $\{(X)_i\}$ are nodal coordinates. The transformation between the global and natural coordinate system for the respective element can be obtained by using Eq. (15).

Consistent with the element shape functions, the displacement/rotation variation along OB can be expressed as function of ξ' as

$$U_y(\xi') = a_0 + a_1\xi' + \cdots + a_{(n-1)}\xi'^{(n-1)} \tag{16a}$$

$$\theta_y(\xi') = a_0 + a_1\xi' + \cdots + a_{(n-1)}\xi'^{(n-1)} \tag{16b}$$

where $f(\xi')$ is a polynomial of order $(n-1)$. The constants $a_0, a_1, \ldots, a_{(n-1)}$ can be evaluated by matching the displacement/rotation conditions at the nodes j, $(j-1), \ldots, (j-n+1)$ in element 1. A set of simultaneous equations of order n is formed, which can be solved for obtaining the constants $a_0, a_1, \ldots, a_{(n-1)}$ related to U_y and θ_y.

Considering element 2, the stress σ_y and moment M_{yy} distribution along OA can be expressed as a function of ξ as

$$\sigma_{yy}(\xi) = b_0 + b_1\xi + \cdots + b_{(n-1)}\xi^{(n-1)} \tag{17a}$$

$$M_{yy}(\xi) = b_0 + b_1\xi + \cdots + b_{(n-1)}\xi^{(n-1)} \tag{17b}$$

where $f(\xi)$ is a polynomial of order $(n-1)$. The constants b_0, $b_1, \ldots, b_{(n-1)}$ can be computed by matching the nodal forces with the derived consistent load vector from finite element analysis. The nodal forces $F_{y,j}, F_{y,(j+1)}, \ldots, F_{y,(j+n-1)}$ and moments $M_{y,j}$, $M_{y,(j+1)}, \ldots, M_{y,(j+n-1)}$ shown in Fig. 3 are the forces and moments exerted at node j, $(j+1), \ldots, (j+n-1)$ by the structure below OA on the structure above OA. In finite element analysis, these forces and moments are obtained by summing up the forces and moments at nodes $j, (j+1), \ldots, (j+n-1)$ from the elements on the side above OA. These forces and moments should be consistent with the stress distribution given in Eq. (17), which can be expressed as

$$F_i = \int_{\Delta a} [N_i]^T \sigma_{yy}(\xi)\, \mathrm{d}x, \qquad i = 1, 2, \ldots, n \tag{18a}$$

$$M_i = \int_{\Delta a} [N_i]^T M_{yy}(\xi)\, \mathrm{d}x, \qquad i = 1, 2, \ldots, n \tag{18b}$$

where N_i are the shape functions of the respective element obtained by substituting $\eta = -1$. By using the transformation between the global and natural coordinate system as given in Eq. (15), $\mathrm{d}x$ can be expressed in terms of $\mathrm{d}\xi$. The integrals given in Eq. (18) can be performed by numerical integration technique. In the present study, the Gauss integration technique has been employed with different orders of integration.

By substituting the expressions for displacement and stress variation given by Eqs. (16) and (17), respectively, in CCI Eq. (12), G_{I} can be expressed as

$$G_{\mathrm{I}} = \underset{\Delta a \to 0}{Lt} \frac{1}{2\Delta a} \int_{\Delta a} \sigma_{yy}(\xi) U_y(\xi')\, \mathrm{d}x \tag{19a}$$

$$G_1 = \underset{\Delta a \to 0}{Lt} \frac{1}{2\Delta a} \int_{\Delta a} M_{yy}(\xi) \theta_y(\xi')\, \mathrm{d}x \tag{19b}$$

On the similar lines the other components of SERR can be expressed as

$$G_{\mathrm{II}} = \underset{\Delta a \to 0}{Lt} \frac{1}{2\Delta a} \int_{\Delta a} \sigma_{xy}(\xi) U_x(\xi')\, \mathrm{d}x \tag{19c}$$

$$G_2 = \underset{\Delta a \to 0}{Lt} \frac{1}{2\Delta a} \int_{\Delta a} Q_z(\xi) W(\xi')\, \mathrm{d}x \tag{19d}$$

$$G_3 = \underset{\Delta a \to 0}{Lt} \frac{1}{2\Delta a} \int_{\Delta a} M_{xy}(\xi) \theta_x(\xi')\, \mathrm{d}x \tag{19e}$$

The integrals given in Eqs. (19) can be performed by numerical integration technique. In the present study, the Gauss numerical integration technique has been employed with the same integration order that is used for evaluating Eq. (18).

NI-MVCCI Technique to Account for Concentric/Eccentric Stiffeners

The same procedure as just given for unstiffened plates is followed for stiffened plates subjected to tensile, bending components and shear loads. However, the following points can be noted with respect to computation of SERR for stiffened plates by using the NI-MVCCI technique:

1) Consider a typical finite element mesh at the crack tip as shown in Fig. 3 indicating the stiffener by dotted line. The stiffener can be concentric or eccentric lying within the plate element in arbitrary position. The stiffness matrix of the respective elements having such stiffeners have to be evaluated by employing MQL9S2 finite element model.

2) For tensile mode I and bending mode 1 fracture, G_{I} and G_1 can be evaluated by multiplying the stress/moment distribution along OA (ahead of crack tip) with the corresponding displacement/rotation distribution along OB (behind crack tip) and integrating this product over Δa. It can be noted that tensile mode I and bending mode 1 fracture are coupled for plates with eccentric stiffeners (G_{I} and G_1), in view of the transformation matrices [Eq. (3)] related to the MQL9S2 finite element model.

3) The stress/moment distribution on the crack extension line OA (expressed in terms of the nodal forces $F_{\mathrm{yp},j}$, $F_{\mathrm{yp},j+1}$, etc., or $M_{\mathrm{yp},j}$, $M_{\mathrm{yp},j+1}$ acting at the nodes j, $j+1$, etc.) and the crack-opening displacement/rotation distribution along OB [expressed in terms of the nodal values at j, $j-1$, $(j-1)'$, etc.] should be evaluated after duly accounting for the stiffener elements in the respective plate finite elements. Let these be represented as σ_{yyp}, σ_{xyp}, M_{yyp}, M_{xyp}, and Q_{zp} and U_{xp}, U_{yp}, U_{zp}, θ_{xp}, and θ_{yp}. The subscript p indicates that stress/moment and displacement components are for that of a stiffened-plate panel evaluated at the plate midsurface level.

4) By substituting the expressions for displacement and stress/moment distributions for a stiffened-plate panel obtained as just described and by using Eq. (19), the components of SERR can be expressed as

$$G_{\mathrm{I}} = \underset{\Delta a \to 0}{Lt} \frac{1}{2\Delta a} \int_{\Delta a} \sigma_{\mathrm{yyp}}(\xi) U_{\mathrm{yp}}(\xi')\, \mathrm{d}x \tag{20a}$$

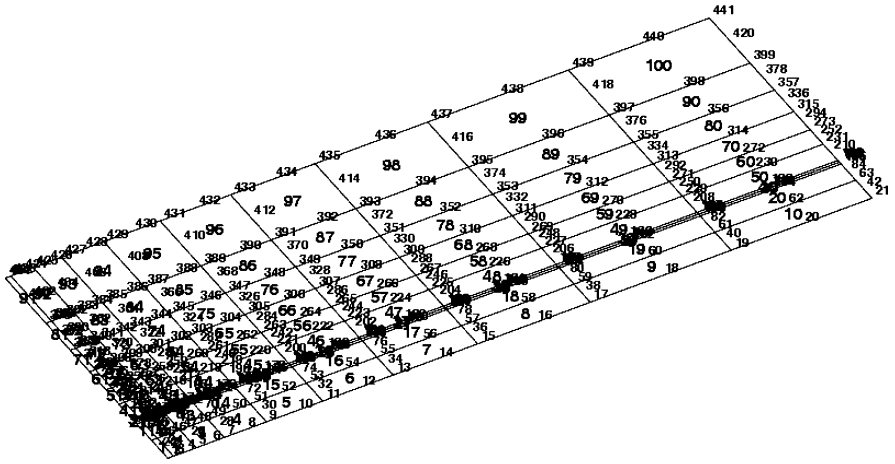

Fig. 4 Finite element idealization of the stiffened plate (quarter symmetry).

$$G_1 = \underset{\Delta a \to 0}{Lt} \frac{1}{2\Delta a} \int_{\Delta a} M_{yyp}(\xi)\theta_y p(\xi')\,dx \tag{20b}$$

$$G_{II} = \underset{\Delta a \to 0}{Lt} \frac{1}{2\Delta a} \int_{\Delta a} \sigma_{xyp}(\xi)U_{xp}(\xi')\,dx \tag{20c}$$

$$G_2 = \underset{\Delta a \to 0}{Lt} \frac{1}{2\Delta a} \int_{\Delta a} Q_{zp}(\xi)w_p(\xi')\,dx \tag{20d}$$

$$G_3 = \underset{\Delta a \to 0}{Lt} \frac{1}{2\Delta a} \int_{\Delta a} M_{xyp}(\xi)\theta_{xp}(\xi')\,dx \tag{20e}$$

5) The integrals given in Eq. (20) can be performed by numerical integration technique. The integrals associated with the evaluation of the constants related to the stress/moment distribution $[b_0, b_1, \ldots, b_{(n-1)}]$ and the preceding integrals are carried out by using Gauss numerical integration technique with an order of three applicable for nine-noded element with assumed transverse shear strain fields.[22]

Numerical Studies

To validate the NI-MVCCI technique just presented, fracture analysis of cracked-stiffened plates subjected to tensile, bending, and shear loads has been conducted by employing the MQL9S2 finite element model. In the example problems illustrated here, material for the stiffener is assumed to be the same as that of the plate, and further it is assumed that the stiffener is continuously attached with the plate. Static analysis of the plates has been conducted by using FEM. The graded finite element idealization of the stiffened plate as shown in Fig. 4 has been chosen for conducting further studies after duly accounting for the stiffener. The finite element idealization is only for the plate, and the presence of stiffener does not increase the total number of degrees of freedom. Fracture analysis has been conducted by employing NI-MVCCI technique for computing SERR and SIF. Gauss numerical integration technique with the three-point rule has been employed for evaluating the integrals associated with NI-MVCCI technique. Plane-strain conditions have been assumed at the crack tip for the example problems to compute SIF by using SERR values.

Example 1: Rectangular Stiffened Plate with Center Crack Under Uniaxial Tension

A free-free rectangular stiffened plate with center crack subjected to uniaxial tensile loading (mode I) as shown in Fig. 5 has been analyzed to compute SERR and SIF at the crack tip. One-quarter of the plate with symmetric boundary conditions has been idealized using MQL9S2 finite element model as shown in Fig. 4. The plate with different crack lengths having $a/W = 0.2$ and 0.3 and with different stiffener cross sections varying from $S_a = 0.0$ to 1.0 ($S_a = A_s/A_p$, where $A_p = t_p^* 2W$) have been considered in the studies. The stiffeners have been considered to be concentric and eccentric with respect

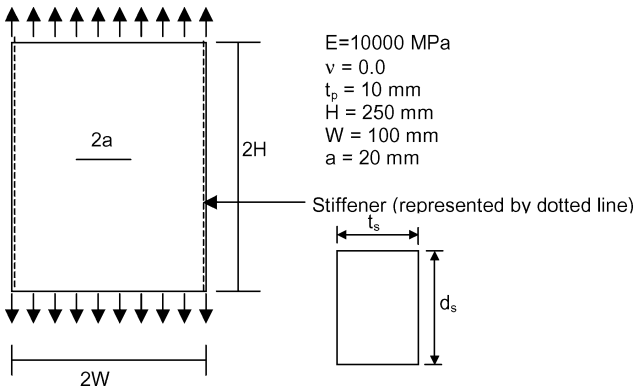

Fig. 5 Rectangular stiffened plate with center crack.

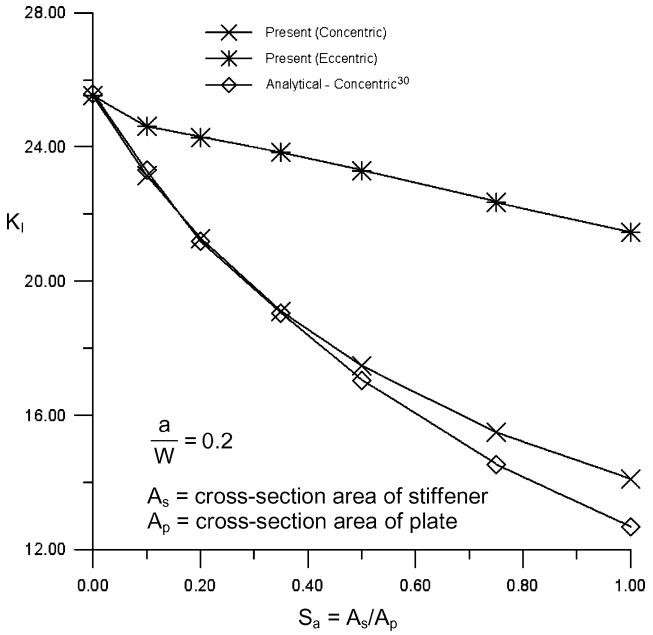

Fig. 6 Variation of K_I with respect to S_a for $a/W = 0.2$.

to the midsurface of the plate. The variation of K_I with respect to S_a for the cases of $a/W = 0.2$ and 0.3 is shown in Figs. 6 and 7, respectively. The results of the present studies have been compared with the available analytical solutions[30] for the case of concentric stiffeners. For the case of eccentric stiffeners, as the tensile loads are applied at the plate midsurface, additional moments are also created because of the eccentricity of loads and the variation of k_1 with respect to S_a for the case of $a/W = 0.2$ and 0.3 shown in Fig. 8.

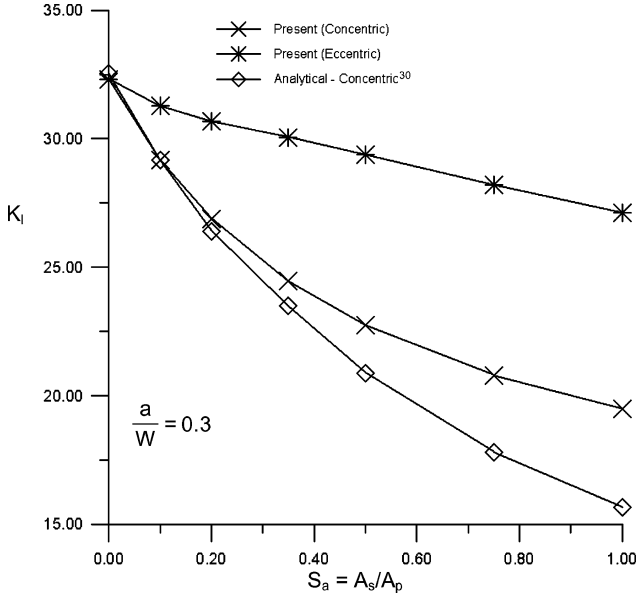

Fig. 7 Variation of K_I with respect to S_a for $a/W = 0.3$.

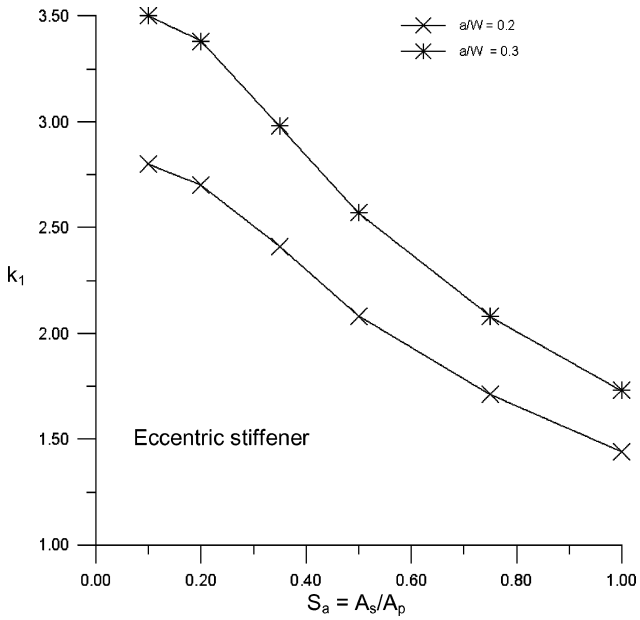

Fig. 8 Variation of k_1 with respect to S_a.

The variation of K_I with respect to a/W for different S_a for the case of concentric and eccentric stiffeners is shown in Figs. 9 and 10, respectively, while the variation of k_1 with respect to a/W for different S_a for the case of eccentric stiffeners is shown in Fig. 11.

Example 2: Rectangular Stiffened Plate with Center Crack Under Tensile-Moment and Tensile-Shear Loads

A free-free rectangular stiffened plate with center crack as shown in Fig. 5 but subjected to uniaxial tensile-moment (modes I and 1) and tensile-shear loads (modes I and 2) has been analyzed to compute SERR and SIF at the crack tip. The geometry and material attribute information for the plate and the stiffener are the same as given in Fig. 5. The same finite element idealization of the plate considering quarter symmetry as shown in Fig. 4 has been used. The plate with different crack lengths having $a/W = 0.1$ to 0.5 and with different stiffener cross sections varying from $S_i = 0.0$ to 1.0 ($S_i = I_s/I_p$) has been considered in the studies. The stiffeners have been considered to be concentric and eccentric with respect to the midsurface of the plate. The variation of K_I and k_1 with respect to

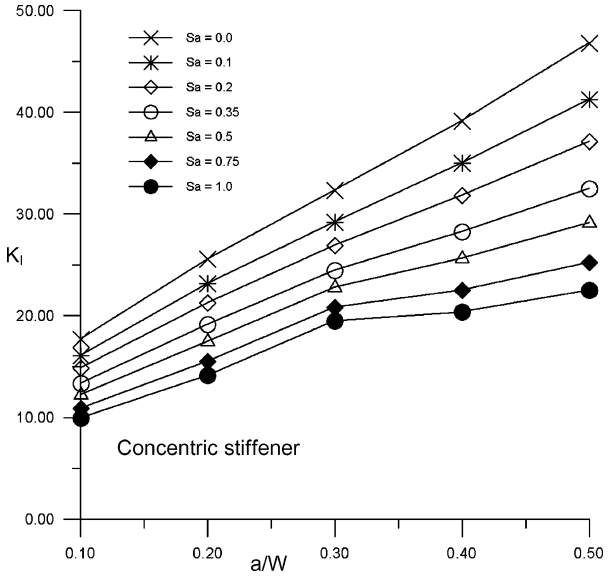

Fig. 9 Variation of K_I with respect to a/W for different S_a.

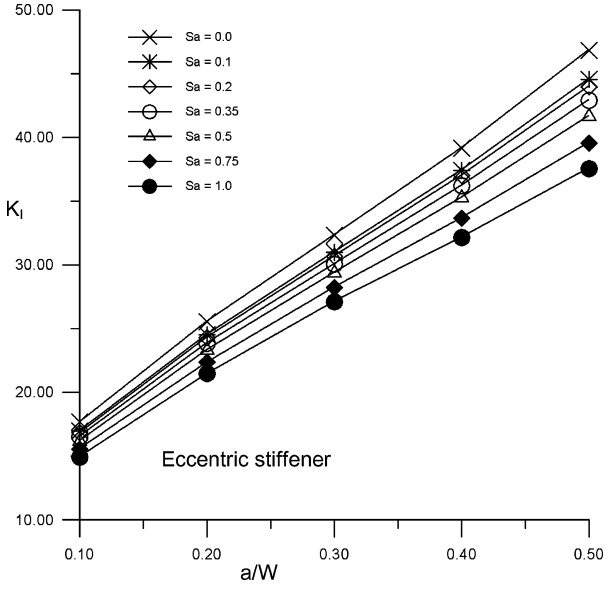

Fig. 10 Variation of K_I with respect to a/W for different S_a.

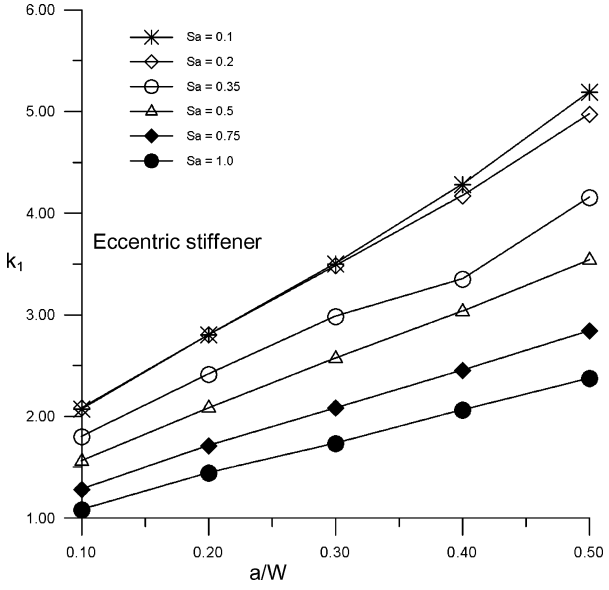

Fig. 11 Variation of k_1 with respect to a/W for different S_a.

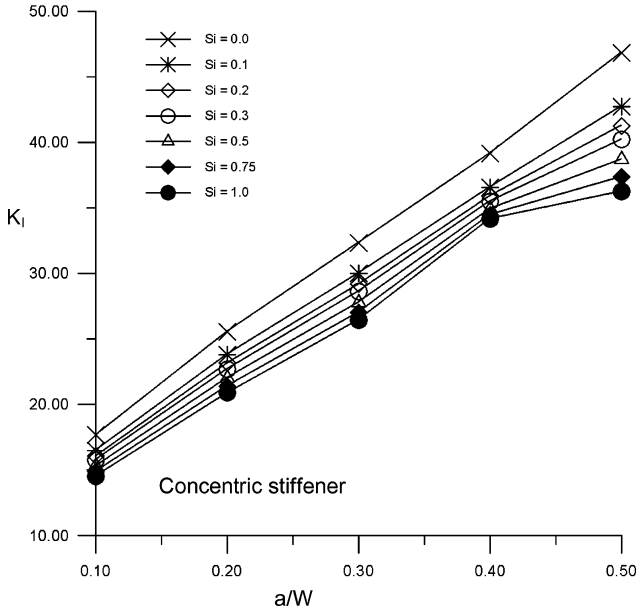

Fig. 12 Variation of K_I with respect to a/W for different S_i (tensile-moment loads).

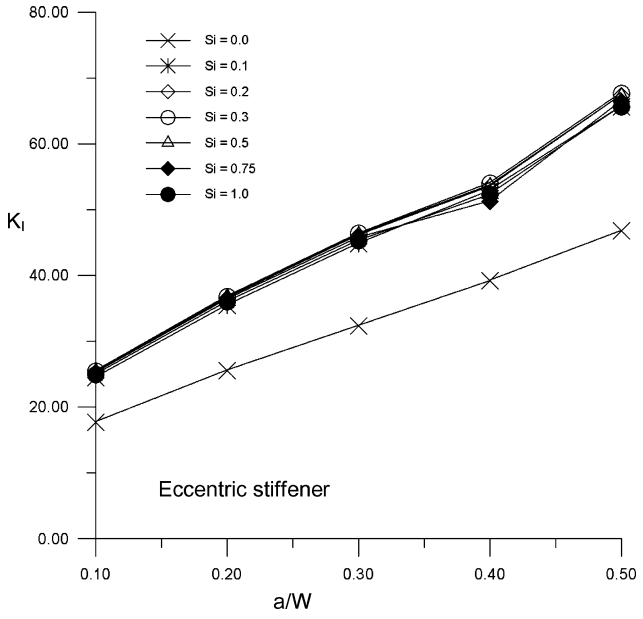

Fig. 13 Variation of K_I with respect to a/W for different S_i (tensile-moment loads).

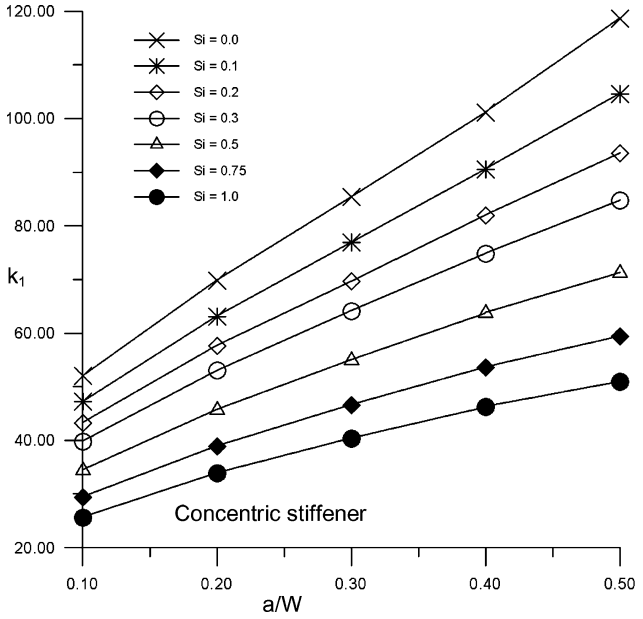

Fig. 14 Variation of k_1 with respect to a/W for different S_i (tensile-moment loads).

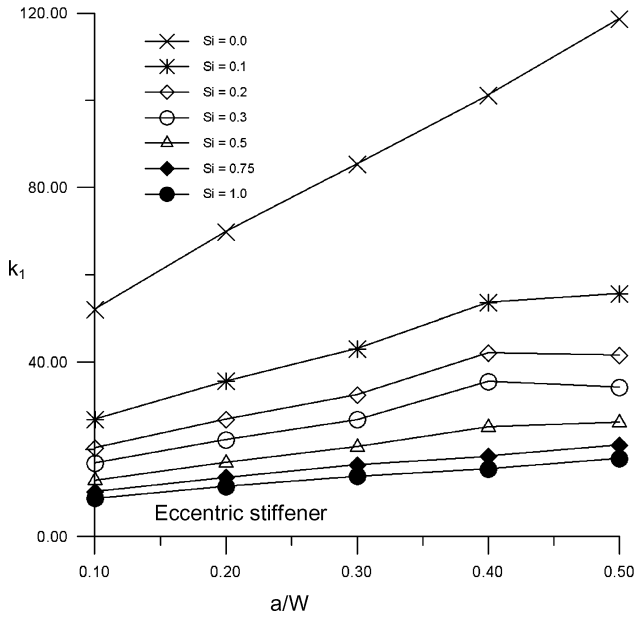

Fig. 15 Variation of k_1 with respect to a/W for different S_i (tensile-moment loads).

a/W for different S_i is shown in Figs. 12–15 for the stiffened-plate panel with concentric and eccentric stiffeners subjected to tensile-moment loads. The variation of K_I and k_2 with respect to a/W for different S_i is shown in Figs. 16–19 for the stiffened-plate panel with concentric and eccentric stiffeners subjected to tensile-shear loads.

Parametric Studies

To demonstrate the application of NI-MVCCI technique just presented, fracture analysis of a free-free rectangular cracked steel stiffened-plate panel subjected to tensile and moment loads as shown in Fig. 20 has been conducted by employing MQL9S2 finite element model. It is decided to consider the plate thickness, the size of the stiffener, and position of the stiffener from the crack tip as the important parameters in conducting the parametric studies. For the plate thickness and the size of stiffeners, standard steel sections available in Indian Standards (IS) steel design tables have been choosen. The stiffeners are considered to be concentric and eccentric with respect to the midsurface of the plate. Fracture analysis has been conducted by using FEM by employing the NI-MVCCI technique for computing SERR and SIF. Gauss numerical integration technique with three-point rule has been employed for evaluating the integrals associated with the NI-MVCCI technique. Plane-strain conditions have been assumed at the crack tip to compute SIF by using SERR values obtained by using the NI-MVCCI technique. SIF values have been normalized in oder to get the nondimensional parameters β_1 and β_1 (geometric/shape factors), corresponding to tensile mode I and bending mode 1. The variation of these nondimensional parameters has been plotted with respect to the other nondimensional parameters α_a or α_i for the different position of the stiffeners. The plot of these variations for the tensile mode I for the case of concentric and eccentric stiffeners has been given in Figs. 21 and 22, respectively. The plot of these variations for the bending mode 1 for the case of concentric and eccentric stiffeners has been given in Figs. 23 and 24, respectively. Polynomial curve fitting has been carried out using MATLAB® software to get a best fit for each of the curves as shown in these plots (Figs. 21–24) corresponding to each of the stiffener positions. The best-fit equations for each of these curves

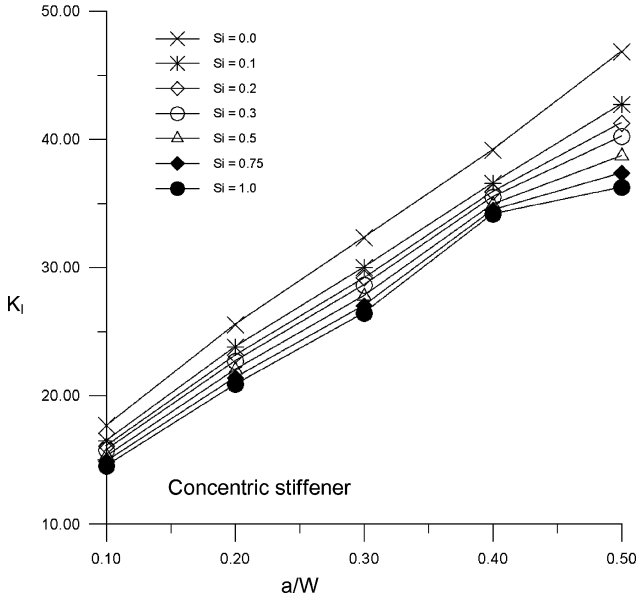

Fig. 16 Variation of K_I with respect to a/W for different S_i (tensile-shear loads).

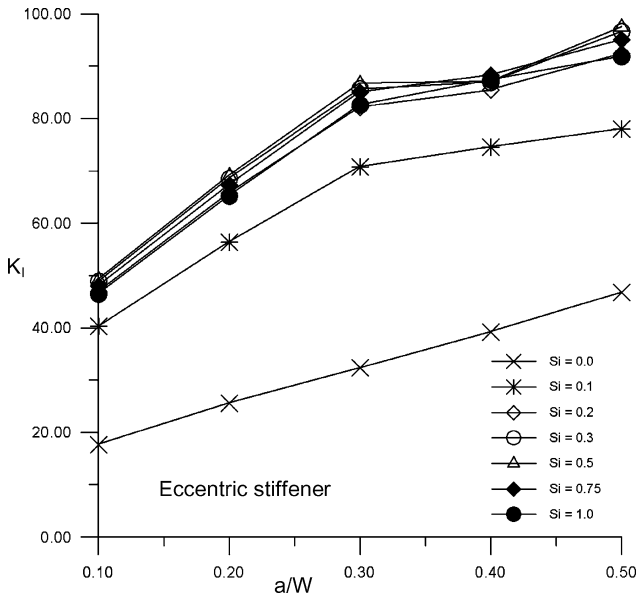

Fig. 17 Variation of K_I with respect to a/W for different S_i (tensile-shear loads).

obtained by using MATLAB software have been given in the Appendix. The error norm obtained for each of these best-fit equations is also indicated.

Discussion of Results

It is observed from Figs. 6 and 7 that SIF values for tensile mode I K_I obtained in the present study for the case of concentric stiffeners are in good agreement with those of the finite-plate solution.[30] It can be observed that for the cases with larger crack lengths (higher a/W ratio) and large size stiffeners ($S_a > 0.9$) SIF values obtained in the present study are overestimated by about 20% compared with the analytical solution. This might be because of the limitation of the MQL9S2 finite element model in terms of representing the stiffness of the very large size stiffeners having an area of about 90% of area of the plate, as the stiffeners are not explicitly modeled in the present formulation. For the stiffened plates with eccentric stiffeners subjected to tensile loads, it can be observed from Figs. 6 and 7 that K_I values are significantly higher (maximum increase of about 30% for $S_a = 1.0$) compared to the case with concentric stiffeners. This is because of the additional moments generated as a result

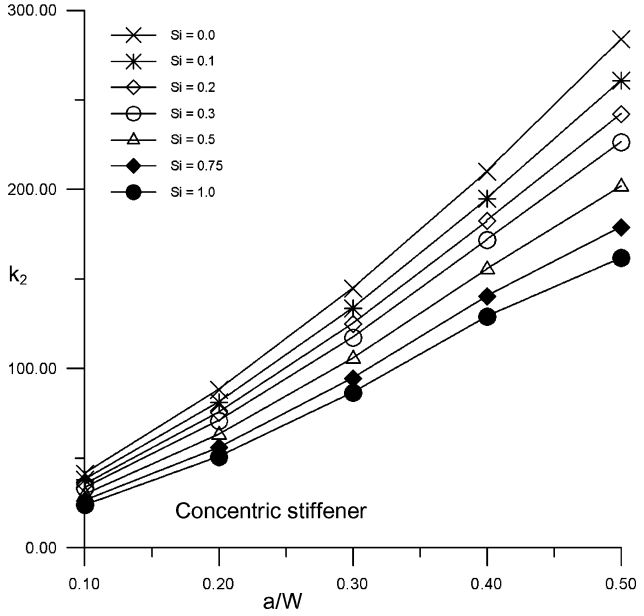

Fig. 18 Variation of k_2 with respect to a/W for different S_i (tensile-shear loads).

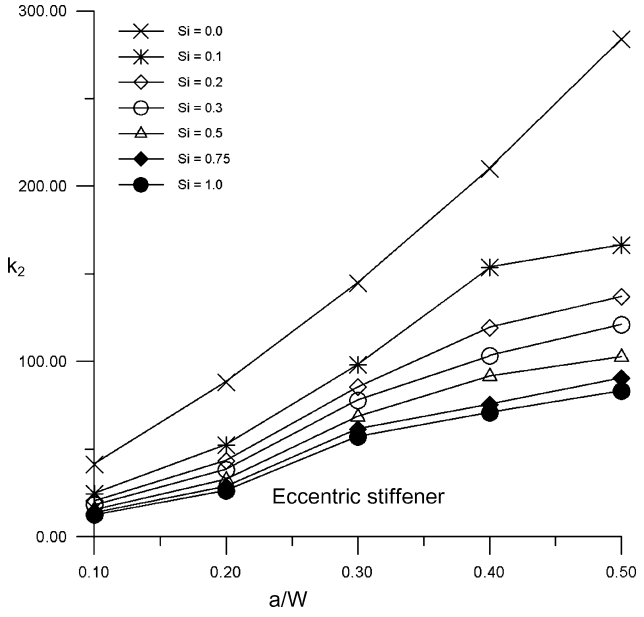

Fig. 19 Variation of k_2 with respect to a/W for different S_i (tensile-shear loads).

of the eccentricity of the tensile loads, which can be observed in Fig. 8 showing SIF values for bending mode 1 k_1 for the eccentric stiffeners. It can be observed from Figs. 6–8 that SIF values for the stiffened plates are consistently lower compared to that of those the unstiffened panel ($S_a = 0.0$).

For the cases with tensile-bending and tensile-shear loads, it can be observed from Figs. 12, 13, 16, and 17 that K_I values for the case with eccentric stiffeners are significantly higher (maximum increase of about 42% for $S_i = 1.0$ for tensile-bending loads and about 212% for $S_i = 1.0$ for tensile-shear loads) compared to those obtained for the case with concentric stiffeners. As already explained, this is because of the additional moments generated as a result of the eccentricity of the tensile loads. It can be observed from Figs. 9, 10, 12, 13, 16, and 17 that variation of K_I with respect to a/W for different S_a or S_i is almost linear for the case of concentric as well as eccentric stiffeners. It can be observed from these figures that the values of K_I decrease with the decreasing a/W values, but for a given a/W value K_I decreases with increasing S_a or S_i values. It can be further observed from Figs. 12, 13, 16, and 17 that K_I values

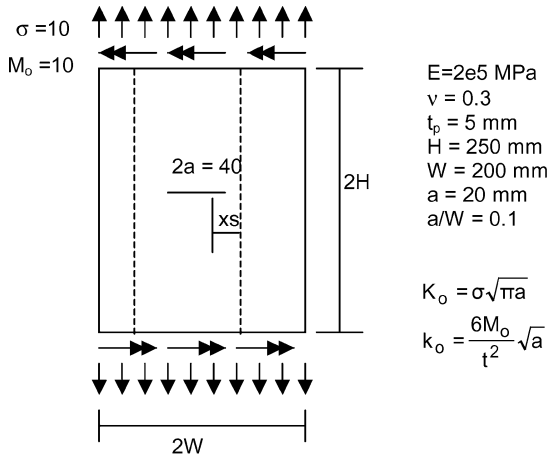

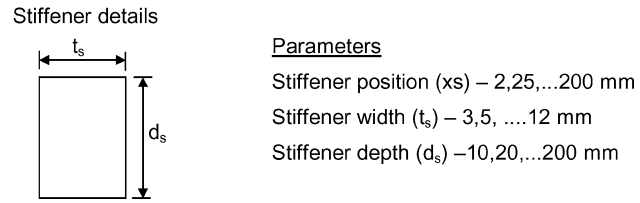

Fig. 20 Stiffened panel with center crack under tensile and moment loads.

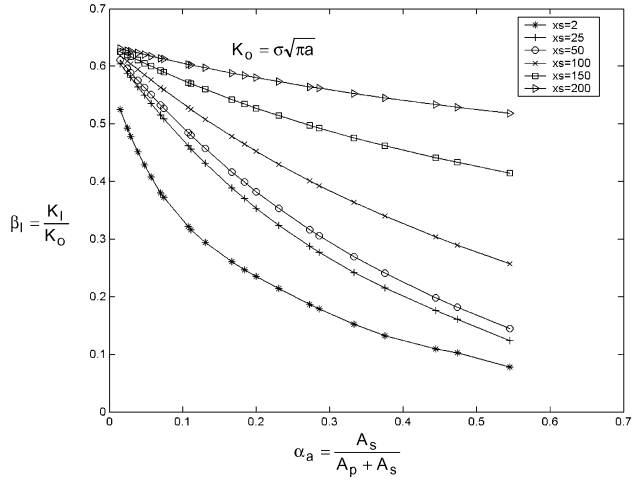

Fig. 21 Variation of β_{I} with respect to α_a for mode I (concentric stiffeners).

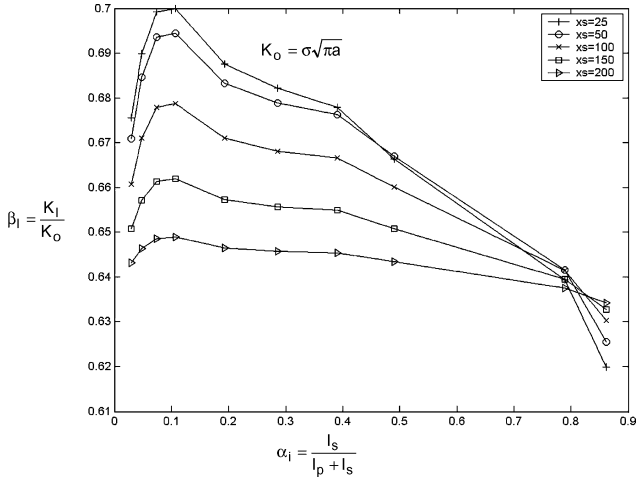

Fig. 22 Variation of β_{I} with respect to α_i for mode I (eccentric stiffeners).

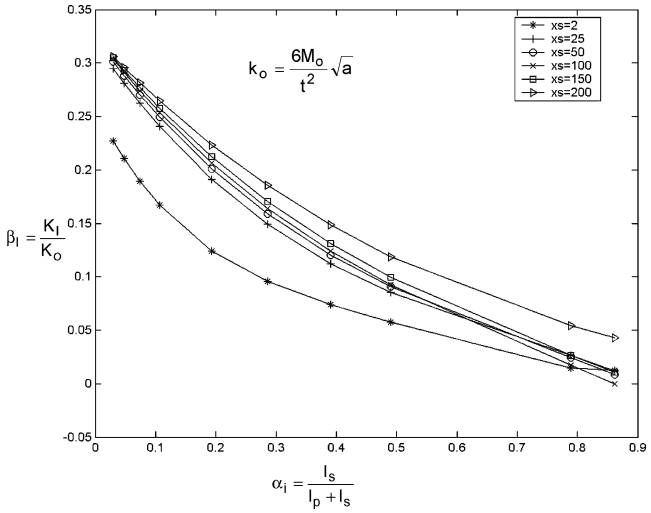

Fig. 23 Variation of β_1 with respect to α_i for mode 1 (concentric stiffeners).

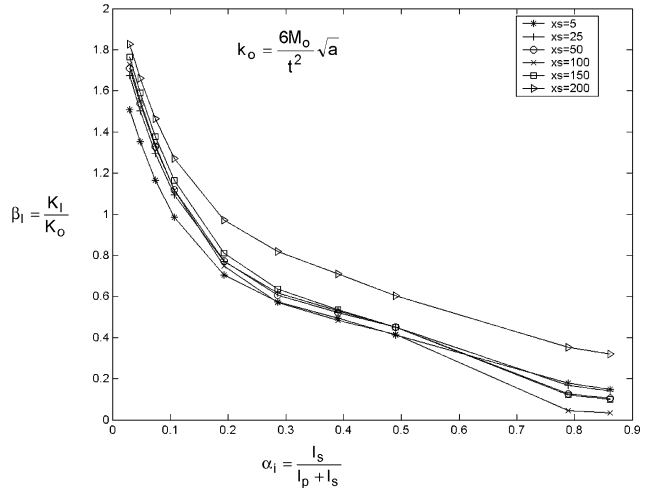

Fig. 24 Variation of β_1 with respect to α_i for mode 1 (eccentric stiffeners).

for the stiffened plates with concentric stiffeners are consistently lower compared to that of the unstiffened planel ($S_i = 0.0$). However, for the stiffened plates with eccentric stiffeners subjected to tensile-bending and tensile-shear loads, K_{I} values are consistently higher compared to that of the unstiffened planel ($S_i = 0.0$). It can be observed from Figs. 14, 15, 18, and 19 that SIF values for bending modes 1 and 2 (k_1 and k_2) are consistently lower compared to that of the unstiffened panel for the cases of concentric as well as eccentric stiffeners. SIF values (k_1 and k_2) for the case with eccentric stiffeners are also lower compared with those obtained for the case with concentric stiffeners. It can be observed from Figs. 12–19 that SIF values for all of the modes (K_1, k_1, and k_2) are consistently increased for increasing a/W for the case with concentric as well as eccentric stiffeners. It can be observed from Figs. 11, 14, and 15 that variation of k_1 with respect to a/W for different S_a or S_i is almost linear for the case of concentric as well as eccentric stiffeners. It can be observed from these figures that the values of k_1 decrease with the decreasing a/W values, but for a given a/W value k_1 decreases with increasing S_a or S_i values. It can be observed from Figs. 18 and 19 that variation of k_2 with respect to a/W for different S_i is almost quadratic for the case of concentric as well as eccentric stiffeners. It can be observed from these figures that the values of k_2 decrease with the decreasing a/W values, but for a given a/W value k_2 decreases with increasing S_i values.

It can be observed from Figs. 21–24 and Eqs. (A1–A4) given in the Appendix that the variation of the nondimensional parameters (β_{I} and β_1) with respect to α_a and α_i follow a particular pattern for the

respective cases, and a best fit of polynomials for each of these cases could be obtained through regression analysis. These equations can be used for computation of SIF values for the corresponding to the position of the stiffener for a given plate and stiffener size without conducting a rigorous finite element analysis. Further parametric studies on typical stiffened plates for different loading cases can be conducted to arrive at similar equations, which will be useful for design against fracture, fatigue crack growth calculations, and for prediction of remaining life of structural components.

Conclusions

NI-MVCCI technique for fracture analysis of cracked-stiffened plates subjected to tensile, moment, and shear loads has been presented. MQL9S2 finite element model obtained by combining nine-noded Lagragian element with assumed shear strain fields with three-noded beam element has been employed. The necessary modification in NI-MVCCI technique to account for concentric and eccentric stiffeners has been discussed. The plate and the stiffener elements are based on Reissner–Mindlin plate theory and Timoshenko beam theory, respectively, which accounts for shear deformations. Based on the numerical studies conducted on cracked-stiffened plates, the following conclusions are drawn:

1) SIF values for tensile mode I K_{I} obtained in the present study for the case of concentric stiffeners are in good agreement with those of the analytical solution available in the literature except for the cases with larger crack lengths (higher a/W ratio) and large-size stiffeners ($S_a > 0.9$). SIF values in such cases obtained in the present study are found to be higher by about 20% compared with the analytical solution. This might be caused by the limitation of the MQL9S2 finite element model in terms of representing the stiffness of the very large size stiffeners having area of about 90% of area of the plate.

2) For the stiffened plates with eccentric stiffeners subjected to pure tensile loads, tensile-bending loads and tensile-shear loads, K_{I} values are generally higher compared to the case with concentric stiffeners. This is because of the additional moments generated as a result of the eccentricity of the tensile loads.

3) K_{I} values for the stiffened plates with concentric stiffeners subjected to pure tensile loads, tensile-bending loads, and tensile-shear loads are consistently lower compared to that of unstiffened panel. However, for the stiffened plates with eccentric stiffeners subjected to tensile-bending loads and tensile-shear loads K_{I} values are consistently higher compared to that of unstiffened planel.

4) SIF values for bending modes 1 and 2, k_1 and k_2, are consistently lower compared to that of the unstiffened panel for the cases of concentric as well as eccentric stiffeners. These values k_1 and k_2 for the case with eccentric stiffeners are also lower compared to those obtained for the case with concentric stiffeners.

5) The variation of K_{I} and k_1 with respect to a/W for different S_a or S_i is almost linear for the case of concentric as well as eccentric stiffeners, while k_2 has quadratic variation with respect to a/W for different S_i.

6) The variation of the nondimensional parameters β_{I} and β_1 with respect to α_a and α_i follow a particular pattern for the respective cases, and a best-fit polynomials for each of these cases could be obtained through regression analysis. These equations can be used for computation of SIF values for the corresponding to the position of the stiffener for a given plate and stiffener size without conducting a rigorous finite element analysis. Further parametric studies on typical stiffened panels for different loading cases can be conducted to arrive at similar equations, which will be useful for design against fracture, fatigue crack growth calculations, and for prediction of remaining life of structural components.

Appendix: Best-Fit Equations

Tensile Mode I (Concentric Stiffeners)

For $xs = 2$,

$$\beta_{\mathrm{I}} = -73.501\alpha_a^5 + 118.377\alpha_a^4 - 73.068\alpha_a^3 + 22.436\alpha_a^2 - 4.125\alpha_a + 0.581 \qquad \text{(error norm} = 0.012267) \quad \text{(A1a)}$$

For $xs = 25$

$$\beta_{\mathrm{I}} = -1.586\alpha_a^3 + 2.510\alpha_a^2 - 1.827\alpha_a + 0.631 \qquad \text{(error norm} = 0.0062756) \quad \text{(A1b)}$$

For $xs = 50$

$$\beta_{\mathrm{I}} = -0.8629\alpha_a^3 + 1.6822\alpha_a^2 - 1.5563\alpha_a + 0.6332 \qquad \text{(error norm} = 0.0062067) \quad \text{(A1c)}$$

For $xs = 100$

$$\beta_{\mathrm{I}} = -0.4843\alpha_a^3 + 0.9982\alpha_a^2 - 1.0924\alpha_a + 0.6348 \qquad \text{(error norm} = 0.0025083) \quad \text{(A1d)}$$

For $xs = 150$

$$\beta_{\mathrm{I}} = -0.3307\alpha_a^3 + 0.6351\alpha_a^2 - 0.6521\alpha_a + 0.6349 \qquad \text{(error norm} = 0.00061437) \quad \text{(A1e)}$$

For $xs = 200$

$$\beta_{\mathrm{I}} = -0.1283\alpha_a^3 + 0.2714\alpha_a^2 - 0.3234\alpha_a + 0.6352 \qquad \text{(error norm} = 0.00068718) \quad \text{(A1f)}$$

Tensile Mode I (Eccentric Stiffeners)

For $xs = 25$

$$\beta_1 = 89.65\alpha_i^7 - 303.8\alpha_i^6 + 412.8\alpha_i^5 - 287.67\alpha_i^4 + 109.04\alpha_i^3 - 21.95\alpha_i^2 + 2.03\alpha_i + 0.633 \qquad \text{(error norm} = 0.0048275) \quad \text{(A2a)}$$

For $xs = 50$

$$\beta_1 = 82.65\alpha_i^7 - 280.4\alpha_i^6 + 382.12\alpha_i^5 - 267.48\alpha_i^4 + 101.93\alpha_i^3 - 20.61\alpha_i^2 + 1.92\alpha_i + 0.621 \qquad \text{(error norm} = 0.0049322) \quad \text{(A2b)}$$

For $xs = 100$

$$\beta_1 = 61.75\alpha_i^7 - 208.87\alpha_i^6 + 284\alpha_i^5 - 198.5\alpha_i^4 + 75.58\alpha_i^3 - 15.29\alpha_i^2 + 1.43\alpha_i + 0.63 \qquad \text{(error norm} = 0.0037079) \quad \text{(A2c)}$$

For $xs = 150$

$$\beta_1 = 36.899\alpha_i^7 - 125.68\alpha_i^6 + 171.99\alpha_i^5 - 120.87\alpha_i^4 + 46.22\alpha_i^3 - 9.37\alpha_i^2 + 0.88\alpha_i + 0.63 \qquad \text{(error norm} = 0.0022657) \quad \text{(A2d)}$$

For $xs = 200$

$$\beta_1 = 19.02\alpha_i^7 - 64.69\alpha_i^6 + 88.471\alpha_i^5 - 62.17\alpha_i^4 + 23.78\alpha_i^3 - 4.83\alpha_i^2 + 0.454\alpha_i + 0.634 \qquad \text{(error norm} = 0.001259) \quad \text{(A2e)}$$

Bending Mode 1 (Concentric Stiffeners)

For $xs = 2$

$$\beta_1 = 1.4699\alpha_i^4 - 3.1712\alpha_i^3 + 2.5486\alpha_i^2 - 1.0647\alpha_i + 0.25587 \quad (\text{error norm} = 0.014637) \quad \text{(A3a)}$$

For $xs = 25$

$$\beta_1 = -0.4335\alpha_i^3 + 0.9064\alpha_i^2 - 0.8143\alpha_i + 0.3178 \quad (\text{error norm} = 0.0068554) \quad \text{(A3b)}$$

For $xs = 50$

$$\beta_1 = -0.3566\alpha_i^3 + 0.7739\alpha_i^2 - 0.7672\alpha_i + 0.3231 \quad (\text{error norm} = 0.0041744) \quad \text{(A3c)}$$

For $xs = 100$

$$\beta_1 = -0.3\alpha_i^3 + 0.6667\alpha_i^2 - 0.7285\alpha_i + 0.3247 \quad (\text{error norm} = 0.0058578) \quad \text{(A3d)}$$

For $xs = 150$

$$\beta_1 = -0.2297\alpha_i^3 + 0.5666\alpha_i^2 - 0.6819\alpha_i + 0.3245 \quad (\text{error norm} = 0.0025905) \quad \text{(A3e)}$$

For $xs = 200$

$$\beta_1 = -0.1233\alpha_i^3 + 0.4130\alpha_i^2 - 0.5895\alpha_i + 0.3230 \quad (\text{error norm} = 0.0040198) \quad \text{(A3f)}$$

Bending Mode 1 (Eccentric Stiffeners)

For $xs = 5$

$$\beta_1 = -24.9994\alpha_i^5 + 73.06\alpha_i^4 - 80.99\alpha_i^3 + 42.515\alpha_i^2 - 11.3838\alpha_i + 1.806 \quad (\text{error norm} = 0.051122) \quad \text{(A4a)}$$

For $xs = 25$

$$\beta_1 = -19.2985\alpha_i^5 + 62.7769\alpha_i^4 - 76.182\alpha_i^3 + 43.109\alpha_i^2 - 12.263\alpha_i + 1.9974 \quad (\text{error norm} = 0.052388) \quad \text{(A4b)}$$

For $xs = 50$

$$\beta_1 = -8.3121\alpha_i^5 + 39.3335\alpha_i^4 - 59.1464\alpha_i^3 + 38.3899\alpha_i^2 - 11.977\alpha_i + 2.0276 \quad (\text{error norm} = 0.056777) \quad \text{(A4c)}$$

For $xs = 100$

$$\beta_1 = 22.3863\alpha_i^4 - 47.701\alpha_i^3 35.6974\alpha_i^2 - 12.0033\alpha_i + 2.0484 \quad (\text{error norm} = 0.061689) \quad \text{(A4d)}$$

For $xs = 150$

$$\beta_1 = -11.1204\alpha_i^5 + 45.1797\alpha_i^4 - 63.1028\alpha_i^3 + 39.373\alpha_i^2 - 12.1543\alpha_i + 2.0856 \quad (\text{error norm} = 0.049805) \quad \text{(A4e)}$$

For $xs = 200$

$$\beta_1 = -29.5998\alpha_i^5 + 83.1355\alpha_i^4 - 88.594\alpha_i^3 + 45.0239\alpha_i^2 - 11.9976\alpha_i + 2.1393 \quad (\text{error norm} = 0.038593) \quad \text{(A4f)}$$

Acknowledgments

Thanks are given to Shri J. Rajasankar, Shri S. Bhaskar, and Shri A. Rama Chandra Murthy, Scientists, Structural Engineering Research Centre (SERC), Chennai, for the useful discussions and suggestions provided during the course of the investigations. This paper is being published with the kind permission of the Director, SERC, Chennai.

References

[1] Schijve, J., "Fatigue of Structures and Materials in the 20th Century and the State of the Art," *International Journal of Fatigue*, Vol. 25, No. 8, 2003, pp. 679–702.

[2] Ratwani, M. M., and Wilhem, D. P., "Influence of Biaxial Loading on Analysis of Cracked Stiffened Panels," *Engineering Fracture Mechanics*, Vol. 11, No. 3, 1979, pp. 585–593.

[3] Shkarayev, S. V., and Moyer, E. T., Jr., "Edge Cracks in Stiffened Plates," *Engineering Fracture Mechanics*, Vol. 27, No. 2, 1987, pp. 127–134.

[4] Shkarayev, S. V., and Moyer, E. T., Jr., "The Effect of Shear and Plasticity on Crack Arrest Characteristics in Stiffened Panels," *Engineering Fracture Mechanics*, Vol. 27, No. 2, 1987, pp. 135–142.

[5] Utukuri, M., and Cartwright, D. J., "Stress Intensity Factors for a Crack near Finite Boundaries in Multiply Stiffened Sheets," *Theoretical Applied Fracture Mechanics*, Vol. 15, No. 3, 1991, pp. 257–266.

[6] Vlieger, H., "The Residual Strength Characteristics of Stiffened Panels Containing Fatigue Cracks," *Engineering Fracture Mechanics*, Vol. 5, No. 2, 1973, pp. 447–477.

[7] Wen, P. H., Aliabadi, M. H., and Young, A., "Stiffened Cracked Plates Analysis by Dual Boundary Element Method," *International Journal of Fracture*, Vol. 106, No. 2, 2000, pp. 245–258.

[8] Isida, M., "On the Determination of Stress Intensity Factor for Common Structural Problems," *Engineering Fracture Mechanics*, Vol. 2, No. 1, 1970, pp. 61–77.

[9] Poe, C. C., "Stress Intensity Factor for a Cracked Sheet with Riveted and Uniformly Spaced Stringers," NASA TR R-358, May 1971.

[10] Wu, B., and Cartwright, D. J., "The Boundary Collocation Method for Stress Intensity Factors of Cracks at Internal Boundaries in a Multiply Stiffened Sheet," *Proceedings of the 3rd International Conference Localized Damage, Computer Aided Assessment and Control*, 1994.

[11] Yashi, O. S., and Shahid, M. M., "The Effect of a Stiffener on a Cracked Plate Under Bending," *International Journal of Pressure Vessel and Piping*, Vol. 23, No. 2, 1986, pp. 133–148.

[12] Yeh, J. R., and Kulak, M., "Fracture Analysis of Cracked Orthotropic Skin Panels with Riveted Stiffeners," *International Journal of Solids and Structures*, Vol. 37, No. 17, 2000, pp. 2473–2487.

[13] Collins, R. A., Cartwright, D. J., and Gregson, P. J., "A Direct Complex Stress Function Approach for Modelling Stiffened Panels Containing Multiple Site Damage," *Theoretical Applied Fracture Mechanics*, Vol. 31, No. 2, 1999, pp. 105–117.

[14] Swift, T., "Fracture Analysis of Stiffened Structure," *Damage Tolerance of Metallic Structures: Analysis Methods and Application*, edited by J. B. Chang and J. L. Rudd, ASTM STP 842, American Society for Testing and Materials, Philadelphia, 1984, pp. 69–107.

[15] Young, A., Rooke, D. P., and Cartwright, D. J., "Analysis of Patched and Stiffened Cracked Panels Using the Boundary Element Method," *International Journal of Solids and Structures*, Vol. 29, No. 17, 1992, pp. 2201–2216.

[16] Young, M. J., and Sun, C. T., "On the Strain Energy Release Rate for a Cracked Plate Subject to Out-of-Plane Bending Moment," *International Journal of Fracture*, Vol. 60, No. 2, 1993, pp. 227–247.

[17] Swift, T., "Development of the Fail Safe Design Features of the DC-10: Damage Tolerance in Aircraft Structures," ASTM STP 486, American Society for Testing and Materials, Philadelphia, 1971, pp. 164–213.

[18] Zaal, K. J. J. M., Van Wimersma Greidanus, B., and Vlot, A., "On the Application of Finite Element Techniques in the Displacement Compatibility Method," *Engineering Fracture Mechanics*, Vol. 52, No. 4, 1995, pp. 625–638.

[19] Dowrick, G., Cartwright, D. J., and Rooke, D. P., "Boundary Effects for a Reinforced Cracked Sheet Using the Boundary Element Method," *Theoretical Applied Fracture Mechanics*, Vol. 12, No. 3, 1990, pp. 251–260.

[20] Young, A., Rooke, D. P., and Cartwright, D. J., "Analysis of Patched and Stiffened Cracked Panels Using the Boundary Element Method," *International Journal of Solids and Structures*, Vol. 29, No. 17, 1992, pp. 2201–2216.

[21] Salgado, N. K., and Aliabadi, M. H., "The Application of the Dual Boundary Element Method to the Analysis of Cracked Stiffened Panels," *Engineering Fracture Mechanics*, Vol. 54, No. 1, 1996, pp. 91–105.

[22] Palani, G. S., Iyer Nagesh, R., and Dattaguru, B., "Fracture Analysis of Cracked Plates Under Tensile, Bending and Shear Loads," *Proceedings of Structural Engineering Convention*, edited by S. K. Bhattacharyya, Indian Inst. of Technology, Kharagpur, India, 2003, pp. 484–491.

[23] Palani, G. S., Iyer Nagesh, R., and Appa Rao, T. V. S. R., "Studies on Performance of Isoparametric Finite Element Models for Static and Vibration Analysis of Eccentrically Stiffened Plates/Shells," Structural Engineering Research Centre, Rept. SST-RR-89-3, Chennai, India, March 1990.

[24]Palani, G. S., Iyer, N. R., and Appa Rao, T. V. S. R., "An Efficient Finite Element Model for Static and Vibration Analysis of Eccentrically Stiffened Plates/Shells," *Computers and Structures*, Vol. 43, No. 4, 1992, pp. 651–661.

[25]Palani, G. S., Iyer, N. R., and Appa Rao, T. V. S. R., "An Efficient Finite Element Model for Static and Vibration Analysis of Plates with Arbitrarily Located Eccentric Stiffeners," *Journal of Sound and Vibration*, Vol. 166, No. 3, 1993, pp. 409–427.

[26]Huang, H. C., *Static and Dynamic Analyses of Plates and Shells; Theory, Software and Applications*, Springer-Verlag, London, 1989.

[27]Irwin, G. R., "Fracture," *Handbook of Physics*, Vol. 6, 1958, pp. 551–590.

[28]Sih, G. C., *Plates and Shells with Cracks*, Noordhoff, Leyden, The Netherlands, 1981.

[29]Viz, M. J., Potyondy, D. O., Zehnder, A. T., Rankin, C. C., and Riks, E., "Computation of Membrane and Bending Stress Intensity Factors for Thin Cracked Plates," *International Journal of Fracture*, Vol. 72, No. 1, 1995, pp. 21–38.

[30]Rooke, D. P., and Cartwright, D. J., *Compendium of Stress Intensity Factors*, Her Majesty's Stationery Office, London, 1976.

B. Sankar
Associate Editor